Effects of Stacking Fault Defects on the X-ray Diffraction Patterns of T2, O2, and O6 Structure $Li_{2/3}[Co_xNi_{1/3-x}Mn_{2/3}]O_2$

Zhonghua Lu[†] and J. R. Dahn*[,†,‡]

Departments of Physics and Chemistry, Dalhousie University, Halifax, Nova Scotia, Canada B3H 3J5

Received November 9, 2000. Revised Manuscript Received March 20, 2001

During the preparation of $Li_{2/3}[Co_xNi_{1/3-x}Mn_{2/3}]O_2$ from $Na_{2/3}[Co_xNi_{1/3-x}Mn_{2/3}]O_2$ by low-temperature ion exchange, the MO_2 sheets slide so the alkali coordination can change from prismatic in the Na compound to octahedral or tetrahedral in the Li compound. All Li-containing samples show stacking faults, some with very high densities of faults, based on broad mixed index peaks in their diffraction patterns. Here, we calculate simulated diffraction patterns using the DIFFaX program developed by Treacy et al. We have considered intergrowths of the T2 and O2 structures and stacking faults in both O2 and O6 structures and have compared the results with experimental X-ray diffraction patterns of $Li_{2/3}[Co_xNi_{1/3-x}Mn_{2/3}]O_2$ ($x = 0$, $^1/_{24}$, and $^1/_{12}$). The stacking fault models are consistent with the experimental data. Furthermore, we suggest that $Li_{2/3}[Co_xNi_{1/3-x}Mn_{2/3}]O_2$ ($x = ^1/_{12}$) is actually a stacking faulted O6 structure, not a stacking faulted O2 structure as we claimed previously.

I. Introduction

Layered alkali transition metal (M) oxides are composed of edge-shared MO_2 sheets with alkali metal atoms sandwiched between them. They can be classified according to the site symmetry of the alkali metal and the way that the MO_2 sheets are stacked. On the basis of the nomenclature developed by C. Delmas and P. Hagenmueller,[1−4] the structures P2 and P3 (with alkali metals in "Prismatic" sites) and the structures O2, O3, and O6 (with alkali metals in "Octahedral" sites) are commonly found. The numeral in the structural designation gives the number of MO_2 sheets in the conventional unit cell. The structures can be distinguished into two groups: (P3 and O3) and (P2, O2, and O6). In the latter group (P2, O2, and O6) the orientation of the MO_2 sheets differs from one layer to its neighbor layers. Structural transitions can occur within each group, via layer translations induced by alkali ion intercalation or ion exchange at low temperature, but not between them.

Recently, during the development of new cathode materials for rechargeable lithium-ion batteries, the T2 (and/or "stacking faulted" O2 or O6) structure $Li_{2/3}[Co_xNi_{1/3-x}Mn_{2/3}]O_2$ phases were obtained[5−11] by ion exchange of Li atoms for Na in the P2 structure $Na_{2/3}[Co_xNi_{1/3-x}Mn_{2/3}]O_2$ ($0 \le x \le ^1/_3$). The designation "T2" indicates that the lithium atoms occupy tetrahedral sites in a material that has a two-layer unit cell. The Li-containing phases have the advantage that they do not convert to the spinel phase, as does O3−$LiMnO_2$, during charge−discharge cycling. When $x = 0$, in the absence of Co substitution, due to the strong superlattice ordering of the transition metal atoms, T2−$Li_{2/3}[Ni_{1/3}Mn_{2/3}]O_2$ can be obtained.[8] As the amount of Co increases, $x \le ^1/_{24}$, the superlattice ordering was weakened and therefore T2−O2 intergrowth structures of $Li_{2/3}[Co_xNi_{1/3-x}Mn_{2/3}]O_2$ were obtained. When $x \ge ^1/_{12}$, it was reported that $Li_{2/3}[Co_xNi_{1/3-x}Mn_{2/3}]O_2$ exists in a stacking faulted O2 structure.[10,11]

The program DIFFaX can be used to simulate powder X-ray diffraction patterns from crystals containing coherent planar stacking faults.[12] This program exploits the recurring patterns found in randomized stacking sequences to compute the average interference wave function scattered from each layer type occurring in a faulted crystal. It has been used to simulate the nature of the stacking faults in orthorhombic $LiMnO_2$[13] as well as many other compounds. In this paper, DIFFaX was

* To whom correspondence should be addressed.
[†] Department of Physics.
[‡] Department of Chemistry.

(1) Delmas, C.; Braconnier, J. J.; Foassier, C.; Hagenmuller, P. *Solid State Ionics* **1981**, *3/4*,165.
(2) Delmas, C.; Braconnier, J.-J.; Maazaz, A.; Hagenmuller, P. *Rev. Chim. Min.* **1982**, *19*, 343.
(3) Delmas, C.; Braconnier, J. J.; Hagenmuller, P. *Mater. Res. Bull.* **1982**, *17*, 117.
(4) Mendiboure, A.; Delmas, C.; Hagenmuller, P. *Mater. Res. Bull.* **1984**, *19*, 1383.
(5) Paulsen, J. M.; Thomas, C. L.; Dahn, J. R. *J. Electrochem. Soc.* **2000**, *147*, 861.
(6) Paulsen, J. M.; Dahn, J. R. *Solid State Ionics* **1999**, *126*, 3.
(7) Paulsen, J. M.; Dahn, J. R. *J. Electrochem. Soc.* **2000**, *147*, 2478.
(8) Paulsen, J. M.; Donaberger, R. A.; Dahn, J. R. *Chem. Mater.* **2000**, *12*, 2257.
(9) Paulsen, J. M.; Thomas, C. L.; Dahn, J. R. *J. Electrochem. Soc.* **1999**, *146*, 3560.
(10) Lu, Z.; Donaberger, R. A.; Dahn, J. R. *Chem. Mater.* **2000**, *12*, 3583.
(11) Lu, Z.; Dahn, J. R. *J. Electrochem. Soc.* **2001**, *148*, A237.
(12) Treacy, M. M. J.; Newsam, J. M.; Deem, M. W. *Proc. R. Soc. London A* **1991**, *433*, 499
(13) Croguennec, L.; Deniard, P.; Brec, R.; Lecerf, A. *J. Mater. Chem.* **1997**, *7*, 511.

10.1021/cm000885d CCC: $20.00
Published on Web 05/15/2001

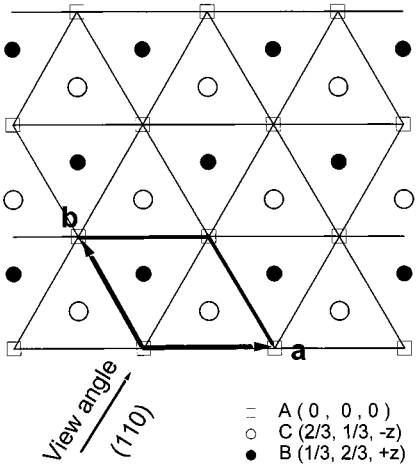

Figure 1. Top view of an MO_2 sheet, showing M atoms on A sites and O atoms on B and C sites. The bold lines indicate the unit cell.

chosen to model the T2−O2 intergrowth and stacking faults in T2/O2/O6 structure $Li_{2/3}[Co_xNi_{1/3-x}Mn_{2/3}]O_2$ ($0 \leq x \leq {}^1/_3$).

II. Using DIFFaX for T2−O2 Intergrowths and Stacking Faults in O2 and O6 Structures

DIFFaX is a modeling, not a refinement, program. To simulate the X-ray diffraction pattern of a stacking faulted structure, one must specify the layers, *i*, that make up the structure as well as the probability, α_{ij}, of finding layer *j* stacked after layer *i*. The interlayer translation vector, $\mathbf{R}_{ij}$, must also be specified.[12] As a first step, we must consider the structures of the perfect P2, O2, T2, and O6 structures.

Layered alkali transition metal oxides, A_xMO_2 (A = alkali metal; M = transition metal) can be assembled from hexagonal close-packed layers of atoms. The transition metals in the structures described here always adopt octahedral coordination between oxygen planes above and below the M atom planes. For example, if the M atoms in an MO_2 sheet occupy the A sites (as shown in Figure 1) in one layer, the O atoms in the neighboring layers can occupy either B (below) and C (above) or C (below) and B (above). The heavy lines in Figure 1 outline the basal plane of the hexagonal unit cell used to describe these structures. If the P2, O2, T2, and O6 structures are viewed along the (110) direction, then the oxygen and transition metal atoms are aligned in rows and the layer stacking sequences are clearly shown as depicted in Figure 2. The alkali metals are not shown in Figure 2 for clarity but also because the X-ray scattering power of alkali metals, such as Li, are very weak and can be ignored for approximate calculations.

The Na atoms in P2 materials occupy trigonal prismatic sites between MO_2 sheets. During ion exchange of Li for Na, neighboring MO_2 sheets slide relative to each other to form octahedral sites for Li because Li prefers to occupy octahedral sites. For the transformation from perfect P2 to perfect O2, every second MO_2 sheet must slide rigidly so that the M atoms move from A sites to B sites. For the transformation from perfect P2 to perfect T2, every second MO_2 sheet must slide so that M atoms move from A sites to positions centered between the M atom hexagons above and below (Figure 2). The T2 structure is stabilized by the stacking of adjacent MO_2 sheets having a strong $\sqrt{3}a \times \sqrt{3}a$ Ni^{2+}−Mn^{4+} superstructure in a manner to minimize Coulomb repulsion.[10] Finally, the formation of O6 from P2 involves a series of translations.

In cases where Co^{3+} has been substituted for Ni^{2+}, the superstructure is weakened[10] and the stability of the T2 phase decreases. Thus, it is natural to expect stacking faulted or intergrowth structures to occur, where a mixture of translations corresponding to O2 and T2 are found in the same structure.

In cases where the superstructure is weak, the tendency is to form O2 or O6 structures. Here, there is a strong likelihood for the appearance of stacking faults. For example, in the formation of perfect O2 from perfect P2, every second layer of MO_2 sheets must slide so the M atoms move from A to B. However, translations where the metal atoms move from A to C are equally efficient at creating octahedral sites for lithium. Stacking faults will naturally occur. Similar arguments can be made about the formation of O6 from P2.

Figure 3 shows an MO_2 sheet at the bottom of the panel. There are only three possible choices for the position of the next MO_2 sheet, and these are indicated. If the M atoms in the layer above are positioned at the sites between B and C, then this is where the layer would be stacked if it were to be in the T2 structure. Let the probability for this to occur be P_t. If the M atoms in the layer above are positioned at the B sites, then this is where the layer would be stacked if it were to be in the O2 structure. Let the probability for this to occur be $P_{O2}(1 - P_t)$. Finally, the M atoms in the layer above could also be positioned at the C site and this will occur with the remaining probability, $(1 - P_{O2})(1 - P_t)$. The same considerations are then made for each of the three possible choices for the second layer to select the position of the third layer. Figure 3 shows the possibilities for the third layer given that the second layer was positioned on the B site. It is clear that if $P_t = 1$, the T2 structure is obtained. If $P_t = 0$ and $P_{O2} = 1$, then the O2 structure is obtained. If $P_t = 0$ and $0.5 \leq P_{O2} < 1$, then stacking faulted O2 structures are obtained. Finally, if $P_t < 1$, then T2−O2 intergrowth structures can be described.

The implementation of the DIFFaX program requires a set of possible layer choices and the translation vectors between them. Figure 4 shows the 12-layer positions that can be used to describe these structures. The layers on the left of Figure 4 are called "type-I" layers here and the layers on the right are called "type-II" layers. In these structures, a type-I layer is always followed by a type-II layer and a type-II layer is always followed by a type-I layer. The fractional atomic coordinates of the atoms in type-I and type-II layers are given in Table 1. Table 2 gives the probabilities for finding layer *j* (shown in Figure 4) located above layer *i* as well as the needed translation vectors, $\mathbf{R}_{ij}$. To be sure that the results in Table 2 describe the needed structures, we compare to Figure 3. The lowest layer in Figure 3 has $i = 1$. The choices for the next layer are $j = 8$, 9, or 10. The second column in Table 2 shows that the probabilities for these choices match those shown in Figure 3.

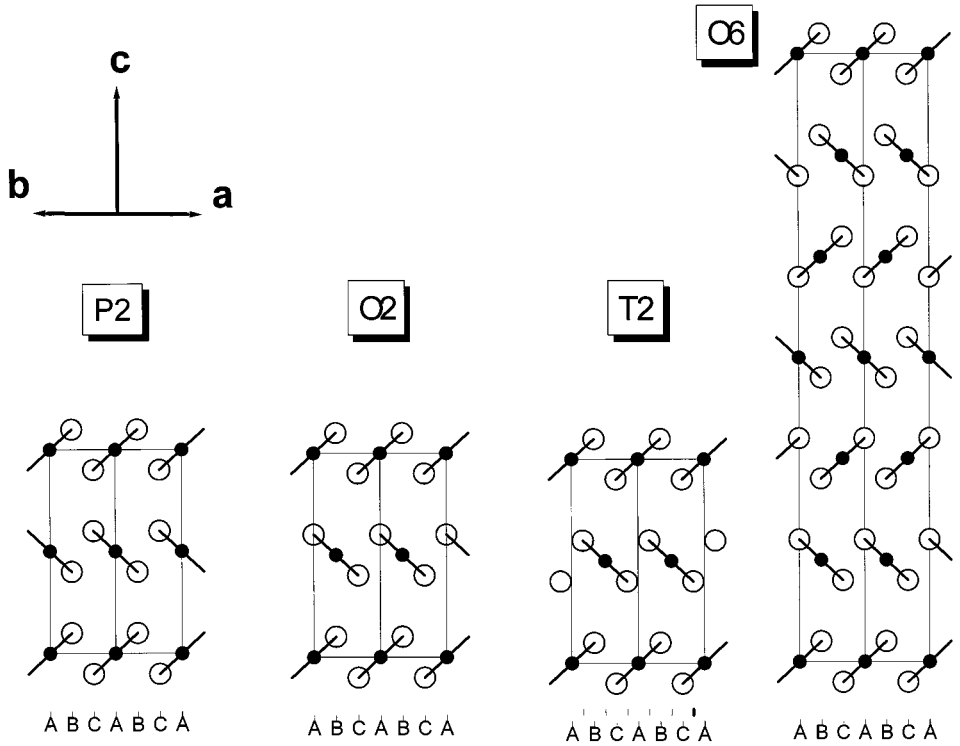

Figure 2. (110) projections of the P2, O2, T2, and O6 structures as indicated.

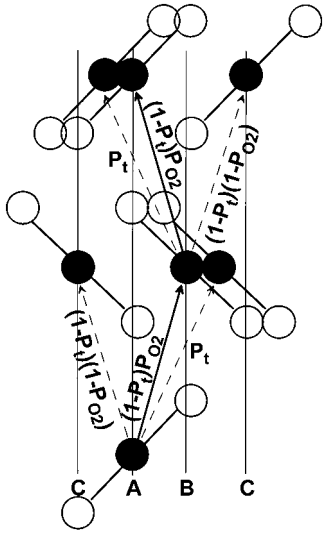

Figure 3. Showing the possible positions of layer 2 above layer 1. The probabilities for each of the three choices are indicated. The possible positions of layer 3 above layer 2, provided layer 2 selects the O2 shift, are also indicated, with their respected probabilities.

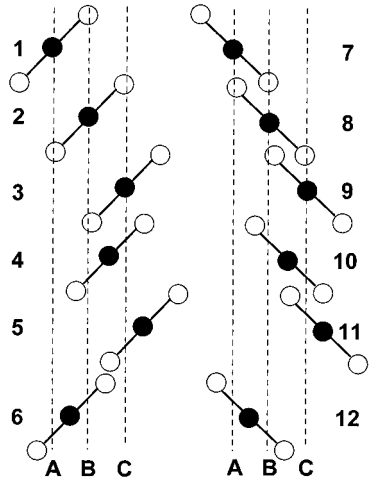

Figure 4. The 12 layers used for the DIFFaX simulation. The layers on the left are "type-I" layers and the layers on the right are "type-II" layers.

The third column in Table 2 is used when O6, stacking faulted O6, and T2-O6 intergrowth structures are desired. It is easy to confirm that the choice $P_t = 0$ and $P_{O6} = 1$ leads to the perfect O_6 structure. We will not illustrate this with detailed diagrams.

III. Results and Discussion

Figure 5 shows the simulated X-ray diffraction patterns for T2−O2 intergrowth structures of MnO_2 sheets. These calculations were made by varying P_t from 0 to 1, with $P_{O2} = 1$. The (10*l*) peaks broaden substantially for $0.1 < P_t < 0.9$, as is typical for stacking faulted structures. Figure 6 shows a direct comparison between the X-ray diffraction patterns of the perfect T2 ($P_t = 1$) and the perfect O2 ($P_t = 0$, $P_{O2} = 1$) structures. Figure 6 clearly shows that the (110) peak is present in both structures while the (111) peak is only present in the T2 structure, as we have indicated before.[7] [Note that the Miller indices are given with respect to the unit cell of the substructure, not taking the Ni−Mn ordering into account.[8]]

Table 1. Atomic Coordination of Layer 1 and Layer 2 ($a = b = 2.86$; $\gamma = 120°$; $c = 5.03$)

	layer I				layer II			
	x	*y*	*z*	occ.	*x*	*y*	*z*	occ.
O(1)	$^1/_3$	$^2/_3$	0.175	1	$^2/_3$	$^1/_3$	0.175	1
Mn	0	0	0	1	0	0	0	1
O(2)	$^2/_3$	$^1/_3$	−0.175	1	$^1/_3$	$^2/_3$	−0.175	1

Table 2. Layer Stacking Probabilities and Stacking Vectors[a]

$i-j$	α_{ij} for T2−O2 and O2 stacking faults	α_{ij} for T2−O6 and O6 stacking faults	$\mathbf{R}_{xij}$	$\mathbf{R}_{yij}$	$\mathbf{R}_{zij}$
1−8	$(1 - P_t)P_{O2}$	$(1 - P_t)P_{O6}$	0.333 33	0.666 67	1.0000
1−9	$(1 - P_t)(1 - P_{O2})$	$(1 - P_t)(1 - P_{O6})$	0.666 67	0.333 33	1.0000
1−10	P_t	P_t	0.500 00	0.500 00	1.0000
2−7	$(1 - P_t)(1 - P_{O2})$	$(1 - P_t)(1 - P_{O6})$	0.666 67	0.333 33	1.0000
2−9	$(1 - P_t)P_{O2}$	$(1 - P_t)P_{O6}$	0.333 33	0.666 67	1.0000
2−11	P_t	P_t	0.500 00	0.500 00	1.0000
3−7	$(1 - P_t)P_{O2}$	$(1 - P_t)P_{O6}$	0.333 33	0.666 67	1.0000
3−8	$(1 - P_t)(1 - P_{O2})$	$(1 - P_t)(1 - P_{O6})$	0.666 67	0.333 33	1.0000
3−12	P_t	P_t	0.500 00	0.500 00	1.0000
4−7	P_t	P_t	0.500 00	0.500 00	1.0000
4−11	$(1 - P_t)P_{O2}$	$(1 - P_t)P_{O6}$	0.333 33	0.666 67	1.0000
4−12	$(1 - P_t)(1 - P_{O2})$	$(1 - P_t)(1 - P_{O6})$	0.666 67	0.333 33	1.0000
5−8	P_t	P_t	0.500 00	0.500 00	1.0000
5−10	$(1 - P_t)(1 - P_{O2})$	$(1 - P_t)(1 - P_{O6})$	0.666 67	0.333 33	1.0000
5−12	$(1 - P_t)P_{O2}$	$(1 - P_t)P_{O6}$	0.333 33	0.666 67	1.0000
6−9	P_t	P_t	0.500 00	0.500 00	1.0000
6−10	$(1 - P_t)P_{O2}$	$(1 - P_t)P_{O6}$	0.333 33	0.666 67	1.0000
6−11	$(1 - P_t)(1 - P_{O2})$	$(1 - P_t)(1 - P_{O6})$	0.666 67	0.333 33	1.0000
7−2	$(1 - P_t)(1 - P_{O2})$	$(1 - P_t)P_{O6}$	0.333 33	0.666 67	1.0000
7−3	$(1 - P_t)P_{O2}$	$(1 - P_t)(1 - P_{O6})$	0.666 67	0.333 33	1.0000
7−4	P_t	P_t	0.500 00	0.500 00	1.0000
8−1	$(1 - P_t)P_{O2}$	$(1 - P_t)(1 - P_{O6})$	0.666 67	0.333 33	1.0000
8−3	$(1 - P_t)(1 - P_{O2})$	$(1 - P_t)P_{O6}$	0.333 33	0.666 67	1.0000
8−5	P_t	P_t	0.500 00	0.500 00	1.0000
9−1	$(1 - P_t)(1 - P_{O2})$	$(1 - P_t)P_{O6}$	0.333 33	0.666 67	1.0000
9−2	$(1 - P_t)P_{O2}$	$(1 - P_t)(1 - P_{O6})$	0.666 67	0.333 33	1.0000
9−6	P_t	P_t	0.500 00	0.500 00	1.0000
10−1	P_t	P_t	0.500 00	0.500 00	1.0000
10−5	$(1 - P_t)(1 - P_{O2})$	$(1 - P_t)P_{O6}$	0.333 33	0.666 67	1.0000
10−6	$(1 - P_t)P_{O2}$	$(1 - P_t)(1 - P_{O6})$	0.666 67	0.333 33	1.0000
11−2	P_t	P_t	0.500 00	0.500 00	1.0000
11−4	$(1 - P_t)P_{O2}$	$(1 - P_t)(1 - P_{O6})$	0.666 67	0.333 33	1.0000
11−6	$(1 - P_t)(1 - P_{O2})$	$(1 - P_t)P_{O6}$	0.333 33	0.666 67	1.0000
12−3	P_t	P_t	0.500 00	0.500 00	1.0000
12−4	$(1 - P_t)(1 - P_{O2})$	$(1 - P_t)P_{O6}$	0.333 33	0.666 67	1.0000
12−5	$(1 - P_t)P_{O2}$	$(1 - P_t)(1 - P_{O6})$	0.666 67	0.333 33	1.0000

[a] Probabilities that are not indicated are zero.

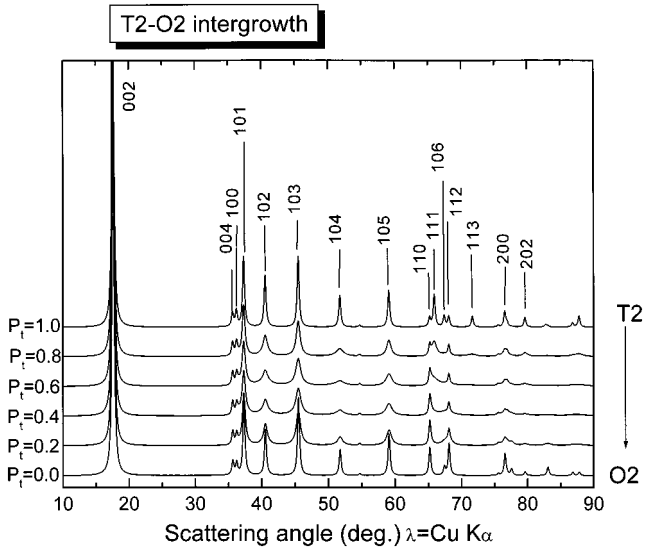

Figure 5. Simulations showing the effect of O2−T2 intergrowth. The calculations were made for $0 < P_t < 1.0$ and $P_{O2} = 1$.

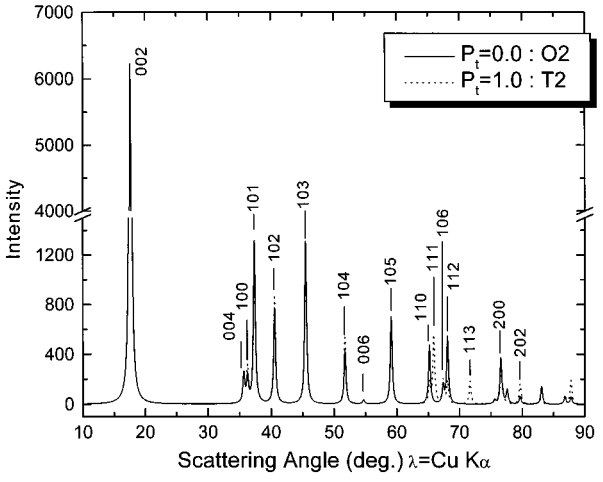

Figure 6. Comparing the diffraction patterns of the pure T2 and pure O2 structures.

To understand why the (111) peak is observed in the T2 structure, but not in the O2 structure, it is necessary to calculate the structure factors for the (111), ($\bar{2}$11), and (1$\bar{2}$1) Bragg peaks that make up the (111) powder peak. For the O2 structure the oxygen sites are ($^1/_3$, $^2/_3$, z), ($^2/_3$, $^1/_3$, $^1/_2 - z$), (0, 0, $^1/_2 + z$), and ($^2/_3$, $^1/_3$, $-z$), and the transition metal sites are (0, 0, 0) and ($^1/_3$, $^2/_3$, $^1/_2$). According to the equation $F_{hkl} = \sum f_j \exp[2\pi i(hx_j + ky_j + lz_j)]$, $F_{\pm(111)} = 0$, $F_{\pm(\bar{2}11)} = 0$, and $F_{\pm(1\bar{2}1)} = 0$. Thus, the (111) peak is not observed for the O2 structure. For the T2 structure the oxygen sites are ($^1/_3$, $^2/_3$, z), ($^1/_6$, $^5/_6$,

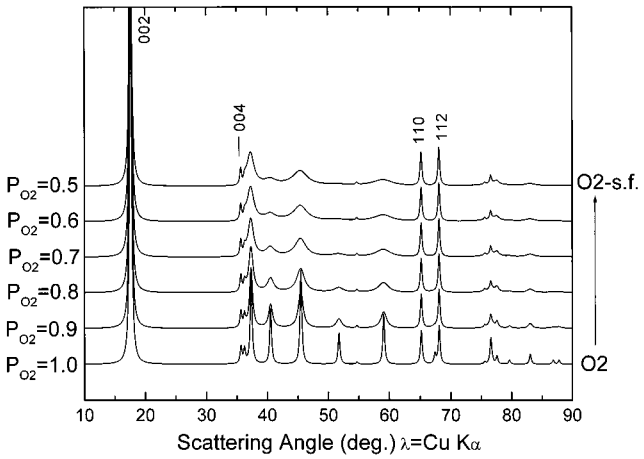

Figure 7. Simulations showing the effect of stacking faults in the O2 structure. The calculations were made for $0.5 \leq P_{O2} \leq 1$ and $P_t = 0$.

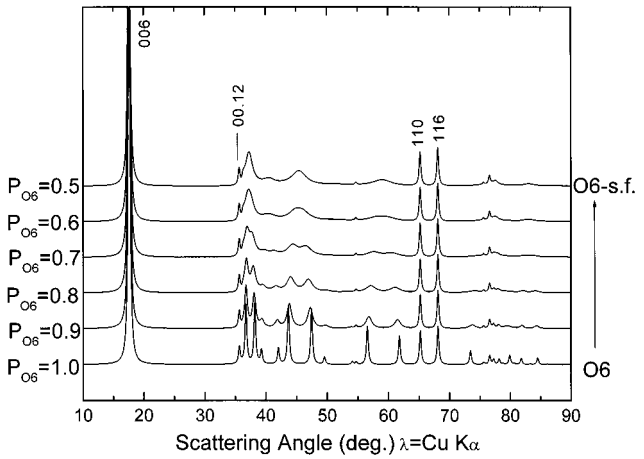

Figure 8. Simulations showing the effect of stacking faults in the O6 structure. The calculations were made for $0.5 \leq P_{O6} \leq 1$ and $P_t = 0$.

$^1/_2 + z$), ($^5/_6$, $^1/_6$, $^1/_2 - z$), and ($^2/_3$, $^1/_3$, $-z$) and the transition metal sites are (0, 0, 0) and ($^1/_2$, $^1/_2$, $^1/_2$). This gives $F_{\pm(111)} = 0$, $F_{\pm(\bar{2}11)} \neq 0$ and $F_{\pm(1\bar{2}1)} \neq 0$. Thus, the (111) peak is observed in the T2 structure.

Figure 7 shows the simulated X-ray diffraction patterns of stacking faulted O2 structures with different contents of stacking faults. These calculations were made with $P_t = 0$ and $0.5 \leq P_{O2} \leq 1$. [The calculations are symmetric over the intervals $0 < P_{O2} < 0.5$ and $0.5 < P_{O2} < 1.0$, so we only present the latter interval.] When the content of stacking faults increases, all peaks except (002), (004), (110), and (112) gradually become broad. Diffraction patterns resembling these have been observed for $Li_{2/3}[M_xMn_{1-x}]O_2$ reported in ref 9.

Figure 8 shows the simulated X-ray diffraction patterns of the O6 structure with different contents of stacking faults. These simulations were made with $P_t = 0$ and $0.5 < P_{O6} < 1$. When the content of the stacking faults increase, all peaks except for (006), (00,12), (110), and (116) become broad. When P_{O6} reaches 0.5, the X-ray diffraction pattern is the same as that in Figure 7 for $P_{O2} = 0.5$, as expected. Now that we have qualitatively predicted the effects of O2−T2 intergrowths and stacking faults in the O2 and O6 structures, we are ready to make a comparison to the experimental results.

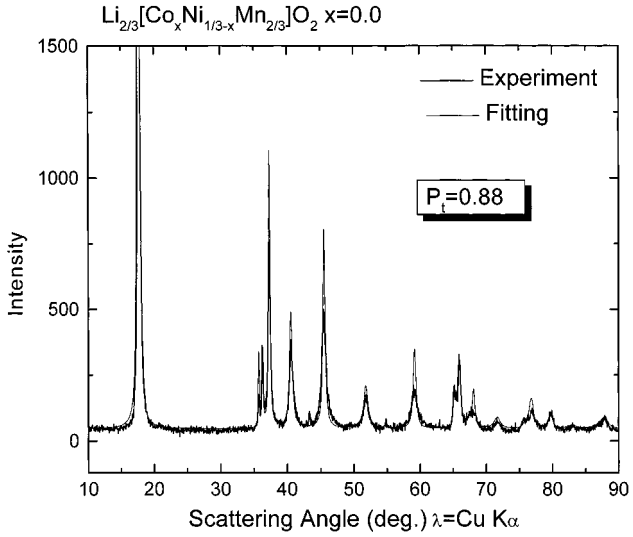

Figure 9. Calculated and experimental diffraction pattern for $Li_{2/3}[Co_xNi_{1/3-x}Mn_{2/3}]O_2$ with $x = 0$. The calculation was made with $P_t = 0.88$, $P_{O2} = 1$, $a = 2.860$ Å, and $c = 5.02$ Å.

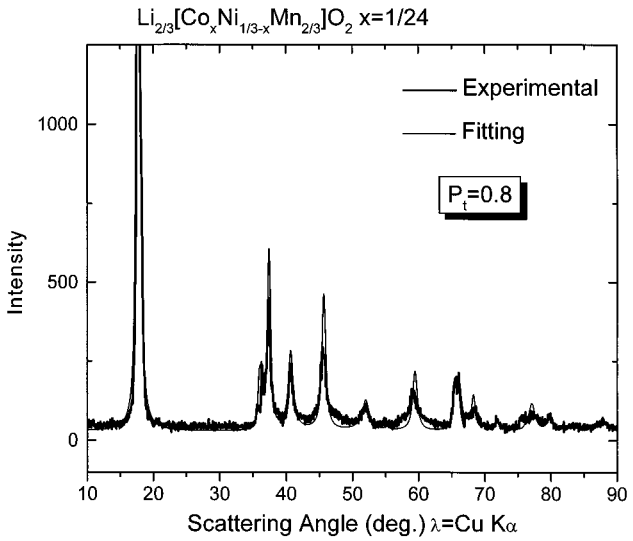

Figure 10. Calculated and experimental diffraction pattern for $Li_{2/3}[Co_xNi_{1/3-x}Mn_{2/3}]O_2$ with $x = {}^1/_{24}$. The calculation was made with $P_t = 0.80$, $P_{O2} = 1$, $a = 2.855$ Å, and $c = 4.99$ Å.

To compare simulated X-ray diffraction patterns with experimental X-ray diffraction patterns of $Li_{2/3}[Co_xNi_{1/3-x}Mn_{2/3}]O_2$, it is necessary to know the lattice parameters a and the interlayer distance c as well as the peak width. Many profile refinement programs express the full width at half-maximum of Bragg peaks as a function of Bragg angle, $\Gamma(\theta)$, as $\Gamma(\theta) = \text{sqrt}(U^* \tan^2(\theta/2) + V^* \tan(\theta/2) + W)$. The adjustable parameters U, V, and W determine the peak width $\Gamma(\theta)$.

The samples described here are the same samples discussed in ref 10. For $x = 0$ and $x = {}^1/_{24}$, $Li_{2/3}[Co_xNi_{1/3-x}Mn_{2/3}]O_2$ exists in the T2−O2 intergrowth structure as shown in Figures 9 and 10, respectively. Each peak of the experimental profile was fitted by a Lorentzian function to extract its peak width, $\Gamma(\theta)$. The variation of $\Gamma(\theta)$ with θ was then fitted to extract reasonable values for U, V, and W, which are then used by the DIFFaX program. The lattice constants were estimated from the positions of the (002) and (110) peaks. The calculated X-ray diffraction patterns assuming T2−O2 intergrowth structures describe the experi-

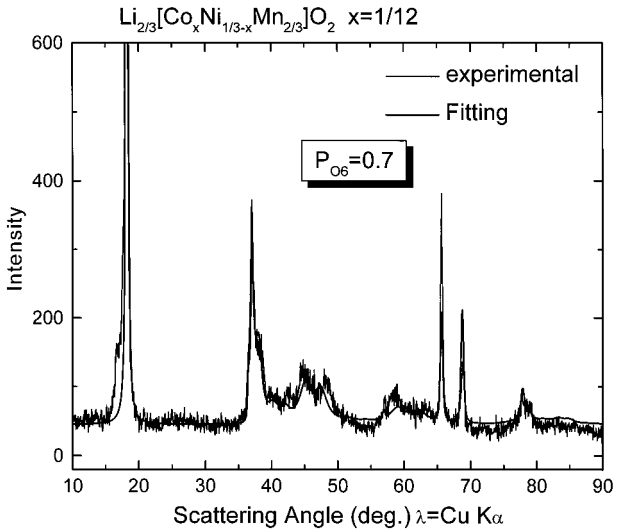

Figure 11. Calculated and experimental diffraction pattern for $Li_{2/3}[Co_xNi_{1/3-x}Mn_{2/3}]O_2$ with $x = {}^1/_{12}$. The calculation was made with $P_t = 0.0$, $P_{O6} = 0.7$, $a = 2.844$ Å, and $c = 4.85$ Å.

mental patterns for $Li_{2/3}[Co_xNi_{1/3-x}Mn_{2/3}]O_2$ with $x = 0$ (Figure 9) and $x = {}^1/_{24}$ (Figure 10) very well. For $x = 0$, we estimate $P_t = 0.88 \pm 0.02$ and for $x = {}^1/_{24}$, we estimate $P_t = 0.80 \pm 0.02$. These estimates are made by the best visual correlation between experiment and simulation.

When the Co doping level reaches $x = {}^1/_{12}$, we stated in ref 10 that $Li_{2/3}[Co_xNi_{1/3-x}Mn_{2/3}]O_2$ is found in a stacking faulted O2 structure. However, a comparison between the experimental profile and the simulations in Figures 7 and 8 suggests that a stacking faulted O6 structure would give a better description of the data. Figure 11 shows that a reasonable description of experiment can be obtained for $P_{O6} = 0.7$ and $P_t = 0$.

IV. Summary

T2−O2 intergrowth structures and stacking fault defects in O2 and O6 structures have been described. Using the DIFFaX software, the X-ray diffraction patterns of T2−O2 intergrowth structures and those of stacking faulted O2 and O6 structures have been simulated. Comparison of the simulations to experimental data for $Li_{2/3}[Co_xNi_{1/3-x}Mn_{2/3}]O_2$ $x = 0$, ${}^1/_{24}$, and ${}^1/_{12}$ shows that good descriptions of the data can be obtained. For $x = 0$ and ${}^1/_{24}$, the structures are described well by T2−O2 intergrowths with $P_t = 0.88$ and $P_t = 0.8$, respectively. For $x = {}^1/_{12}$, the structure is well-described by a stacking faulted O6 structure with $P_t = 0$ and $P_{O6} = 0.7$, not a stacking faulted O2 structure as we claimed in ref 10.

It is most likely that the electrochemical properties of $Li_{2/3}[Co_xNi_{1/3-x}Mn_{2/3}]O_2$ will depend not only on the stoichiometry of the compound but also on the nature of the stacking fault defects. Now that we can understand the nature of the stacking faults, at least semi-quantitatively, we are optimistic that we can understand the variation of electrochemical properties of these materials with their complex structures. This will be the subject of future work.

Acknowledgment. The authors acknowledge the support of 3M Co., 3M Canada Co., NSERC, and NRC for the funding of this work.

CM000885D